Progress In Electromagnetics Research M, Vol. 13, 53–68, 2010

BROADBAND MEASUREMENT OF COMPLEX PERMITTIVITY OF COMPOSITE AT MICROWAVE FREQUENCIES USING SCALAR SCATTERING PARAMETERS

S. Borah and N. S. Bhattacharyya

Microwave Engineering Laboratory
Department of Physics
Tezpur University
Tezpur, Assam-784 028, India

Abstract—A shielded, conductor-backed coplanar waveguide technique is used to determine the complex permittivity and loss tangent of nano magnetic composite materials over X-band. The test composite material is synthesized by reinforcing cobalt ferrite particles with average crystallite diameter 7.36 nm in low density polyethylene matrix with 2% and 4% volume fractions. The complex permittivity for low density polyethylene matrix and the composite samples, evaluated from the present technique at 9.887 GHz, are verified with cavity perturbation technique resonating at the same frequency. A new mathematical approach, using element-to-element correspondence of the ABCD matrix, is applied to calculate the complex propagation constant. The formulation facilitates evaluation of complex propagation constant over the test frequency range using scalar scattering parameters without altering the coplanar waveguide geometry. The mathematical formulation is verified by performing permittivity measurements for air over the X-band.

1. INTRODUCTION

Broadband device applications make it essential to measure the complex permittivity of materials over a wide range of frequencies. The methods for material property characterizations at microwave frequencies are based on transmission lines and the resonant structures developed from transmission lines [1–5]. Nonresonant methods, using coaxial lines and rectangular waveguides, are suitable for characterizing

Corresponding author: N. S. Bhattacharyya (nidhisbhatta@gmail.com).

samples of fixed thickness. Techniques employing microstrip and coplanar lines, however, allow characterizing samples of varying thickness. Resonant methods are, essentially, limited to single frequency or its harmonics, whereas, the broadband characterization of the dielectric properties of material is possible using nonresonant methods [6]. The broadband measurements can be realized by optimizing the shape of the microstrip or coplanar geometry to allow propagation of dominant quasi-TEM mode [3]. The broadband extraction can be performed using stripline, microstrip line and waveguide as feeding structures [7–13]. This can be realized either by using the test samples as substrate or by placing it over the structure whose substrate properties is known. Some pioneer work on broad-band measurements of complex permittivity are reported by

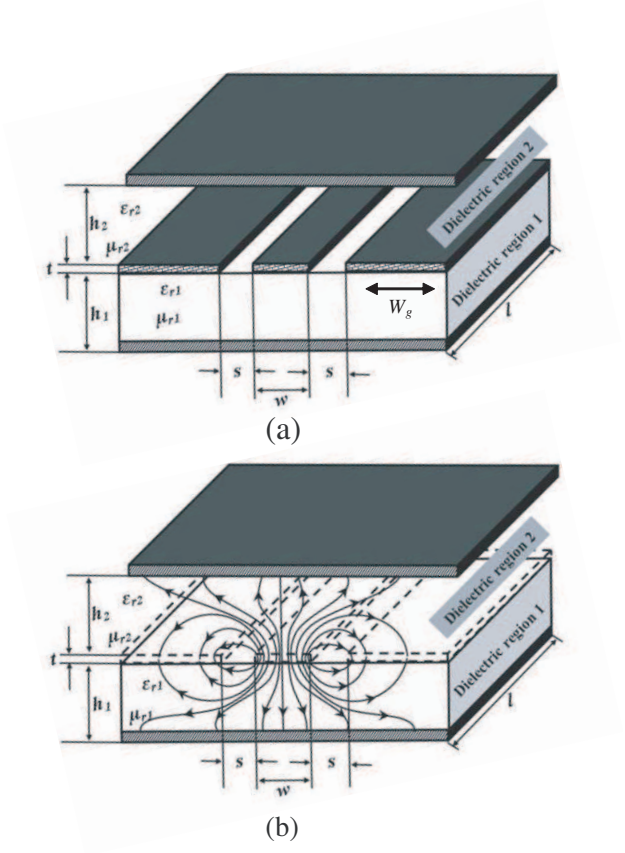

Figure 1. (a) Schematic of shielded conductor-backed coplanar waveguide configuration. (b) Electromagnetic field distribution in shielded conductor-backed coplanar waveguide structure.

Weir [14], Barry [15] and Hu et al. [16] using complex S-parameters. However, these techniques employ vector measurements and, thus, usually need complex instrumentation. Non-resonant techniques require full electromagnetic modelling of the measurement geometries for precise determination of permittivity at microwave frequencies. In references [17, 18], scalar measurement technique is reported which is employed only for planar four-port microwave device.

In the present investigation, a simple mathematical approach has been developed to evaluate the complex permittivity using scalar S-parameters over broad microwave frequency range, using single conductor-backed CPW geometry. A shielded conductor-backed CPW structure, Fig. 1(a), is used to determine the complex permittivity of magneto-polymer composite material. Nano sized cobalt ferrite in low density polyethylene matrix ($CoFe_2O_4$-LDPE) is synthesized as test composite material. Magneto-dielectric properties of the composite material can be tailored to miniaturize the size of the microwave devices designed on it. In addition, external magnetic tuning can be used for enhancing bandwidth of operation of the device. Fast relaxing cobalt ion in the ferrite at microwave frequencies makes it as potential material for microstrip substrate application [19–21]. From the measured scalar S-parameters, complex propagation constant is computed using element-to-element correspondence of the ABCD matrix. Here transmission (ABCD) matrix solutions are determined considering conductor-backed CPW as two port network [22].

2. CONDUCTOR-BACKED CPW DESIGN CONSIDERATION

The geometry used in the present investigation is a conventional coplanar waveguide (CPW) with conductor backing and top metal cover. Unshielded CPW, without conductor backing, is a three-conductor line with finite lateral ground planes and single centre strip. The structure can generate two fundamental quasi-TEM modes — even mode and odd mode with zero cut-off frequency [23]. The even mode, commonly known as coplanar waveguide mode, is generated when the two lateral ground planes have equal potential. The odd mode, also called as slotline mode, is generated when the two lateral ground planes are of equal magnitude but different potentials. Apart from the above modes, in unshielded CPW with conductor backing, parasitic modes similar to microstrip like surface wave mode may be generated, even if lateral ground planes and the back conductor are at same potential. The parasitic mode excited inside conductor-backed coplanar waveguide depends on the height of the substrate and

geometrical line parameters. This mode propagates together with the even and odd modes for normal CPW [24]. In quasi-static analysis technique, the influence of the odd mode and the surface wave mode is not considered [25]. Since our formulation is based on quasi-static analysis, the design parameters of the conductor-backed CPW are optimized to suppress the occurrence of the unwanted modes. The design considerations are based on full wave analysis available in the literature [16, 22–28].

Suppression of odd modes is accomplished by keeping the lateral ground planes at equal potential. Equal potential can be achieved by putting air bridges, but at times this may lead to floating potential. In the conductor-backed CPW structure used, the lateral ground planes and conductor backing is kept at the same ground potential by means of properly spaced conductive side bridges [24].

Height and width of the strip are important dimensions of conductor-backed CPW, which decide whether the radio frequency transmission through the structure follow microstrip (parasitic mode) or coplanar line (even mode) configuration. For a fixed substrate thickness, h_1, as the width, w, of the signal conductor increases the ratio of guided wavelength to free space wavelength (λ_g/λ_0), approaches that of a microstrip line. On the other hand, for a fixed w as h_1 increases, the ratio λ_g/λ_0, approaches that of a conventional CPW. For low dispersion, the separation, s, of the lateral ground conductor and the signal conductor is chosen such that $h_1 > w + 2s$ and $h_1 \leq \lambda/2$. This criterion makes the even mode propagation as quasi-TEM dominant mode [16].

Upper metal shield results in reduction of line impedance only. To lessen the effect of shield height, h_2, on the line impedance, minimum value of h_2 should be about two times that of $2s + w$ for CPW without conductor-back. Conductor-backed coplanar lines are relatively less sensitive to shielding than free-standing coplanar waveguides, for the same characteristic impedance. Thus the criterion $h_2 \geq 1.5(2s + w)$ is a good approximation for practical design [26].

There are four limiting cases of electromagnetic field distribution for the conductor-backed CPW with a top metal cover, as mentioned in reference [27]. Here, a normal electromagnetic field distribution in conductor-backed CPW is considered. To ensure the electromagnetic propagation through shielded conductor-backed CPW, similar to normal CPW, the top metal cover height h_2 is kept comparable to the substrate thickness h_1 (Fig. 1(b)).

Coplanar lines with lateral ground planes of unequal widths and unequal slot widths, additionally, have the tendency to excite the unwanted odd mode on the waveguide and, therefore, are not used in

the conductor-backed CPW design. The lateral ground-plane width, W_g, is chosen to fulfil the condition $W_g \geq 0.5(2s+w)$, so that the effect of the ground width on the characteristic impedances of the even and the odd mode can be neglected [26].

3. FORMULATION

The procedure for the evaluation of the complex permittivity involves two steps [16]. First is the calculation of the filling factors through conformal mapping. The second step involves deriving a relation for determining the complex permittivity of the test material in terms of the characteristic impedance and propagation constant of the conductor-backed CPW configuration using S-parameters.

3.1. Calculation of Filling Factors

For the structure shown in Fig. 1(a), the two filling factors, q_1 and q_2 for the dielectric region 1 and 2 of the conductor-backed CPW configuration, respectively, can be derived using conformal mapping technique [24, 28], as follows

$$q_1 = \frac{\frac{K(k_1)}{K(k_1')}}{\frac{K(k_1)}{K(k_1')} + \frac{K(k_2)}{K(k_2')}} \tag{1}$$

$$q_2 = \frac{\frac{K(k_2)}{K(k_2')}}{\frac{K(k_1)}{K(k_1')} + \frac{K(k_2)}{K(k_2')}} \tag{2}$$

where

$$k_1 = \tanh(\pi w/4h_1) \Big/ \tanh\{\pi(2s+w)/4h_1\} \tag{3}$$

$$k_2 = \tanh(\pi w/4h_2) \Big/ \tanh\{\pi(2s+w)/4h_2\} \tag{4}$$

with $K(k)$ and $K(k')$ being the elliptic integrals of the first kind and its complement, and $k_i' = \sqrt{1-k_i^2}$.

3.2. Calculation of Complex Permittivity

The scattering parameters of the test structure are converted to ABCD parameters by the following relation

$$\begin{bmatrix} A & B \\ C & D \end{bmatrix} = \frac{1}{2S_{21}} \begin{bmatrix} (1+S_{11})(1-S_{22})+S_{12}S_{21} & Z_0\{(1+S_{11})(1+S_{22})-S_{12}S_{21}\} \\ \frac{1}{Z_0}\{(1-S_{11})(1-S_{22})-S_{12}S_{21} & (1-S_{11})(1+S_{22})+S_{12}S_{21} \end{bmatrix} \tag{5}$$

The ABCD parameters for the conductor-backed CPW structure of length, l, can be expressed in terms of the propagating parameters of the transmission line as [16, 22]

$$\begin{bmatrix} A & B \\ C & D \end{bmatrix} = \begin{bmatrix} \cosh(\gamma l) & \mathrm{Z}_e \sinh(\gamma l) \\ \frac{1}{Z_e}\sinh(\gamma l) & \cosh(\gamma l) \end{bmatrix} \tag{6}$$

where Z_e and γ are the characteristic impedance and complex propagation constant of the transmission line, respectively. From (5), the characteristic impedance and propagation constant can be expressed in terms of the known experimental ABCD parameters and the length of the coplanar waveguide. An ambiguity does result in the propagation constant due to electrical length being unknown, this can be resolved by keeping the length of the conductor-backed CPW less than half a wavelength long.

The challenge is to determine γ over a broad band of frequency using scalar S-parameters and keeping the same conductor-backed CPW geometry. Equations (5) and (6) shows that A, B, C and D are complex quantities. However, in our measurements the S-parameters are scalar. To incorporate our measurements to evaluate ABCD, those frequencies have to be taken, for which either $\alpha = 0,\ \beta \neq 0$ or $\alpha \neq 0,\ \beta = 0,\ \pi$ is satisfied. This limits the determination of the complex propagation constant, γ, to certain values of frequency for those lengths of the conductor-backed CPW structure, which satisfies the condition of phase constant, $\beta = 0$ or π. Consequently, for a complete sweep of frequency, different guided wavelengths have to be considered and, hence, different conductor-backed CPW structures.

To overcome the above constrain, γ is computed over a broad frequency range after mathematically simplifying (6) by element-to-element correspondence of the ABCD matrix and considering $Z_0 \cong 50\,\Omega$. Equation (6) can be rewritten as

$$\begin{bmatrix} A & B \\ C & D \end{bmatrix} = \begin{bmatrix} \cos(j\gamma l) & -jZ_e \sin(j\gamma l) \\ -\frac{j}{Z_e}\sin(j\gamma l) & \cos(j\gamma l) \end{bmatrix} \tag{7}$$

Thus from (7),

$$-j\left[Z_e \sin(j\gamma l) + \frac{1}{Z_e}\sin(j\gamma l)\right] = B + C \tag{8}$$

$$-j\sin(j\gamma l) = \frac{B+C}{Z_e + {}^1\!/_{Z_e}} \tag{9}$$

The characteristic impedance Z_e of the transmission line is given as

$$Z_e = \sqrt{{}^B\!/_C} \tag{10}$$

From (9) and (10)

$$j\gamma l = \sin^{-1}\left[j\left(\frac{B+C}{\sqrt{B/C}+\sqrt{C/B}}\right)\right] \tag{11}$$

$$\gamma = \alpha + j\beta = \frac{-j}{l}\sin^{-1}(j\xi), \text{ where } \xi = \frac{B+C}{\sqrt{B/C}+\sqrt{C/B}} \tag{12}$$

and is computed from the measured scalar S-parameters.

Effective relative permittivity with the test material is calculated from the expression

$$\varepsilon^*_{reff} = \frac{Z_{e\_V}\gamma}{\omega Z_e\sqrt{\varepsilon_0\mu_0}} \tag{13}$$

where ω is angular frequency and Z_{e_V} is the characteristic impedance when the test material (dielectric region 2) is replaced with free space ($\varepsilon_0 = 8.845\times10^{-12}$ F/m, $\mu_0 = 4\pi\times10^{-7}$ H/m) and can be found from

$$Z_{e\_V} = \frac{60\pi}{\sqrt{\varepsilon_{eff}}}\frac{1}{\frac{K(k_1)}{K(k_1')}+\frac{K(k_2)}{K(k_2')}} \tag{14}$$

Accurate expressions for the ratio $K(k)/K(k')$ are available in [29].

The effective permittivity ε_{eff} of the substrate w.r.t. air can be calculated from

$$\varepsilon_{eff} = 1 + q_1(\varepsilon_{r1}-1) \tag{15}$$

where ε_{r1} is the permittivity of the known material (dielectric region 1).

Finally, the complex permittivity, ε^*_{r2}, of the unknown material is determined by substituting the values of ε^*_{reff} from (13) in the equation given below [16]

$$\varepsilon^*_{r2} = \varepsilon'_{r2} - j\varepsilon''_{r2} = \varepsilon'_{r2}(1 - j\tan\delta_e) = \frac{\varepsilon^*_{reff}}{q_2} - \frac{q_1\varepsilon_{r1}}{q_2} \tag{16}$$

4. METHODOLOGY

4.1. Fabrication of the Conductor-backed CPW Configuration

The conductor-backed CPW is fabricated over a glass epoxy substrate with known permittivity $\varepsilon_{r1} = 4.5$ and $h_1 = h_2 = 2.4$ mm. The coplanar strip dimensions $s = 0.19$ mm and $w = 1.2$ mm are chosen such that, $h_1 > w + 2s$ and $h_2 \geq 1.5(2s + w)$. The lateral ground-plane width, W_g, is chosen as 0.84 mm. To satisfy the condition $l < \lambda/2$ for X-band operation, the length of the coplanar strip is taken as

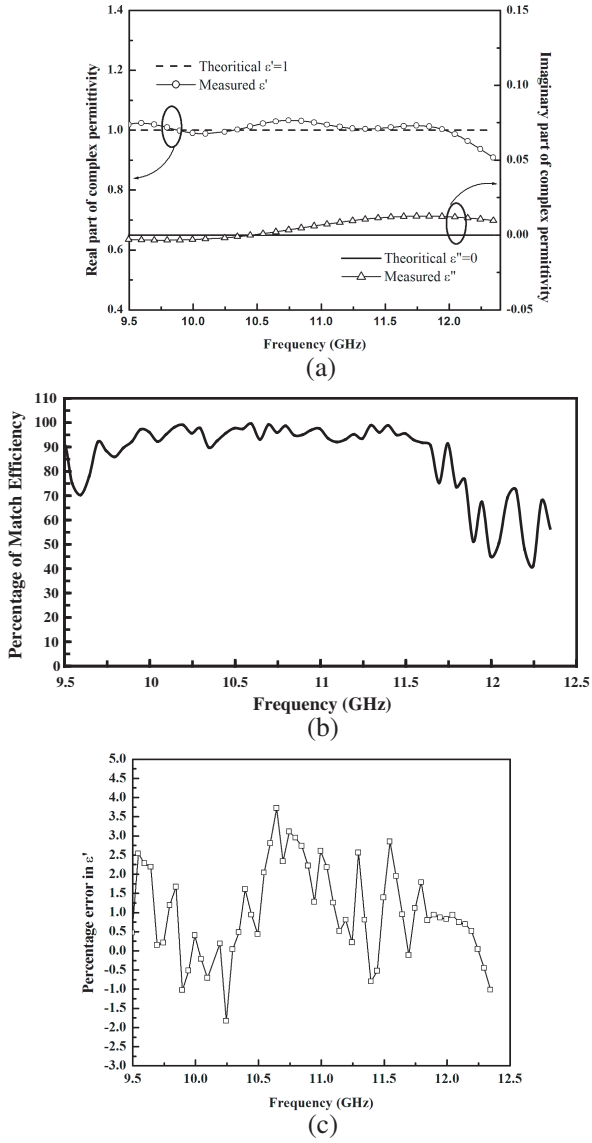

Figure 2. (a) Real and imaginary part of complex permittivity of air over X-band. (b) Percentage of match efficiency of the conductor-backed coplanar waveguide structure. (c) Percentage of in the real part of permittivity during calibration with air.

13 mm. The coplanar waveguide structure is fabricated with 50 Ohm coaxial impedance matching. The filling factors are calculated using (1) and (2). The scalar S-parameters are measured using an automated PC-based system developed in the laboratory [30]. Measurements are carried out over a range from 9.500 to 12.045 GHz, as the impedance mismatch becomes more pronounced beyond 12.045 GHz (Fig. 2(b)).

4.2. Test Material Synthesis

Particulate magneto-polymer composite is used as the test material for the complex permittivity measurement in this method. Nano sized ferrite particles are prepared by wet synthesis method [31] by dissolving iron (III) nitrate and cobaltous nitrate in stoichiometric proportion in deionised water, oleic acid and sodium hydroxide (3 M, 20 ml) and stirred at 80°C. The polycrystalline residue is annealed at 400°C for three hours to get cobalt ferrite particles. Homogenous composite of LDPE with $CoFe_2O_4$ is fabricated by reinforcing 2% and 4% volume fractions (V.F.) of $CoFe_2O_4$ in LDPE, dissolved in cyclohexane at 70°C. The test samples are fabricated by moulding the composite to rectangular shapes with thickness varying from 0.5 mm–1.0 mm. X-ray diffraction, Transmission Electron Microscopy and Scanning Electron Microscopy studies confirm cubic spinel structure of the ferrites and their uniform distribution in the matrix. The average crystallite diameter of the ferrite particles is found to be $\cong 7.36$ nm.

5. RESULTS AND DISCUSSIONS

5.1. Calibration of the Conductor-backed CPW

In order to validate the measurement technique, experimental measurements for the conductor-backed CPW configuration are carried out repetitively with air.

Filling the dielectric region 2 with air, the complex permittivity is obtained over the X-band frequencies using this technique. The experimental values agree quantitatively with the theoretical value $\varepsilon_{air} = 1 + j0$ [32].

A marginal deviation, with root mean square error equal to 0.0158 in the complex permittivity of air, from the theoretical value is observed (Fig. 2(a)). The maximum percentage error in measurement of $\varepsilon'(\Delta\varepsilon')$ is found to be ranging from -1.83% to $+3.72\%$ as shown in Fig. 2(c).

5.2. Mismatch Analysis

The conductor-backed CPW structure is designed considering 50 Ohm impedance matching (referred in Section 4.1). Practical fabrication may lead to impedance mismatch over the range of frequencies under consideration and, hence, may affect the complex permittivity results. The possible mismatch error can occur in all the S-parameters. However, $|S_{12}|$ parameter of the test sample is taken w.r.t. direct power (dielectric region 2 as air). Thus, the $|S_{12}|$ mismatch error does not effect computation of effective relative permittivity and the mismatch error can be considered due to $|S_{11}|$ (or $|S_{22}|$). $|S_{11}|$ is equal to $|S_{22}|$, as conductor-backed CPW configuration is symmetric. The mismatch is computed taking dielectric region 2 as air and is found out in terms of percentage of match efficiency using

$$\eta_{match}\,(\%) = 100 \times \left(1 - |S_{11}|^2\right) \tag{17}$$

Figure 2(b) shows the impedance mismatch.

5.3. Complex Permittivity Measurement of the Test Samples

The dielectric region 2 of the conductor-backed CPW configuration is filled, alternatively by LDPE, 2% and 4% VF $CoFe_2O_4$-LDPE composite as test materials. The measurements are carried out at room temperature over 9.500 GHz to 12.045 GHz and complex permittivity is computed using (16).

Figures 3(a) and 4(a) show material dispersion analogous to Barry [15], with maximum coupling in the conductor-backed CPW structure at 10 GHz, as seen from the prominent peaks within 9.7 GHz–10.4 GHz. However, on increasing the resolution of the permittivity spectra along y-axis [Fig. 3(b)], ε' of LDPE shows variation through 9.500 GHz to 12.045 GHz. Analysis of propagation of electromagnetic waves through non-conductors can explain the variation of complex permittivity with frequency [33]. Electrons in a dielectric molecule, considered to be situated at different locations, experiences different natural angular frequencies and damping. If f_i bounded electrons, with frequency ω_i, mass m and damping γ_i in each molecule interact with the electromagnetic wave of angular frequency ω, then the polarization $\mathbf{P}$ is given by

$$\mathbf{P} = \mathrm{Re}(\mathbf{P}^*) = \mathrm{Re}\left[\frac{Nq^2}{m}\left(\sum_i \frac{f_i}{\omega_i^2 - \omega^2 - j\gamma_i\omega}\right)\mathbf{E}^*\right] \tag{18}$$

where the system has N molecules per unit volume.

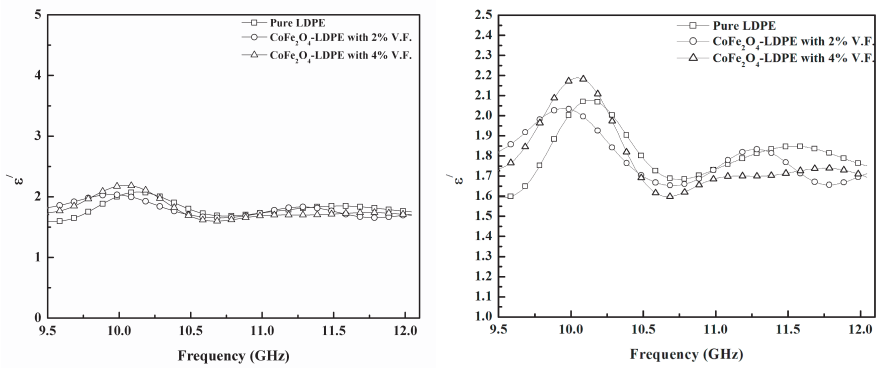

Figure 3. Permittivity spectra of $CoFe_2O_4$-LDPE composite with 2% and 4% volume fractions compared with pure low density polyethylene: (a) real part of the complex permittivity (ε') and (b) permittivity axis with increased resolution.

LDPE has a chain structure with side branches and are oriented in different directions in bulk polymer. When pumped with microwave power with varying ω, the dipole moment and hence, the polarization of the molecules fluctuates in accordance with (13). Complex polarization $\mathbf{P}^*$ is also related to complex field $\mathbf{E}^*$ by relation, $\mathbf{P}^* = \varepsilon_0 \chi_e^* \mathbf{E}^*$, where χ_e^* is the complex susceptibility. The complex permittivity is given by $\varepsilon^* = \varepsilon_0(1+\chi_e^*)$ and the relative complex permittivity is determined by relation

$$\varepsilon_r^* = 1 + \frac{Nq^2}{m\varepsilon_0} \sum_i \frac{f_i}{\omega_i^2 - \omega^2 - j\gamma_i\omega} \tag{19}$$

Hence from (19) both real and imaginary part of relative complex permittivity of the system will vary with the frequency of pumped electromagnetic wave. A resonance may occur when the frequency of electron ω_i equals ω, resulting in maximum value of real part of ε_r^*, which in present investigation is at 10.13 GHz for LDPE. This phenomenon remains even after reinforcement of LDPE with the particulate fillers. Fillers in composites will also have electrons having different locational natural frequencies and damping and hence different interacting frequency with pumped microwave, leading to variation in ε' values of the composites. Here, in $CoFe_2O_4$-LDPE composites, the resonance frequency is found ranging between 9.7 GHz–10.4 GHz.

A similar variation is observed on increasing the resolution of

the loss tangent ($\tan\delta_\varepsilon$) spectra along y-axis [Fig. 4(b)]. However, above 10 GHz, losses of the composite material are found to be lower than that of pure LDPE and are attributed to electron hopping phenomenon, which gets restricted in the composite [34].

To substantiate complex permittivity of the test material at microwave frequencies, dielectric measurements are carried out using cavity perturbation technique [2]. A TE_{103} reflection cavity at 9.887 GHz with Q value of 1832.35 is fabricated for measurements. Affirmation of results are done on pure LDPE (as reference material) using both cavity perturbation and conductor-backed CPW technique. The results obtained are tabulated in Table 1. The value of ε' for pure LDPE, measured with the cavity perturbation technique, varies in the range 1.85–2.57 at 9.887 GHz. It is comparable to the standard value of permittivity of LDPE at X-band which is 2.26 [35]. The variation in the permittivity values in cavity perturbation technique is because the measurement system has a frequency least-count of 0.001 GHz [30] and cannot precisely resolve frequency shifts less than that. It is observed from Table 1 that the values of real part of complex permittivity and loss tangent of the test samples obtained from both the techniques are comparable.

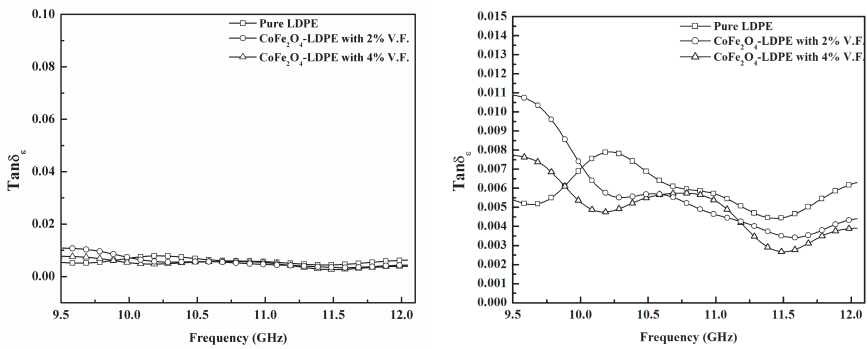

Figure 4. Dielectric loss tangent spectra of $CoFe_2O_4$-LDPE composite with 2% and 4% volume fractions compared with pure low density polyethylene: (a) loss tangent of the complex permittivity ($\tan\delta_\varepsilon$) and (b) loss tangent axis with increased resolution.

Table 1. Complex permittivity of the pure LDPE and $CoFe_2O_4$-LDPE composite with 2% and 4% V.F. of filler at 9.887 GHz.

		At 9.887 GHz			
		Cavity perturbation technique		Conductor-backed CPW technique	
	% VF of filler	ε'	$\tan\delta_\varepsilon$	ε' ($\Delta\varepsilon'$ = –0.54%)	$\tan\delta_\varepsilon$ ($\Delta\tan\delta_\varepsilon$ = ±0%)
Pure LDPE	0	1.85-2.57	0.0059-0.0061	1.904	0.0062
$CoFe_2O_4$-LDPE	2	1.87-2.07	0.0062-0.0082	2.035	0.0086
$CoFe_2O_4$-LDPE	4	1.92-2.14	0.0060-0.0078	2.082	0.0059

6. CONCLUSION

In this work, the computational approach is modified making it possible to determine complex permittivity over a wide range of frequencies using scalar S-parameters, without incorporating any changes in the geometry. The technique is versatile, non-destructive and can also be used to simultaneously extract complex permittivity and permeability. In addition, the technique requires a simple calculation and calibration procedure in terms of scalar measurements and avoids expensive vector measurements. The technique is limited by the thickness of the test material which has to be comparable with the thickness of the substrate of the CPW structure.

REFERENCES

1. Hajian, M., K. T. Mathew, and L. P. Ligthart, "Measurement of complex permittivity with waveguide resonator using perturbation technique," *Microwave and Optical Technology Letters*, Vol. 21, 269, 1999.
2. Murthy, V. R. K., S. Sunderam, and B. Viswanathan, *Microwave Materials*, 100, Narosa Publishing House, 1990.
3. Chen, L. F., C. K. Ong, C. P. Neo, V. V. Varadan, and V. K. Varadan, *Microwave Electronics Measurement and Material*

Characterization, 37, John Willey and Sons, West Sussex, England, 2004.

4. Yamashita, E., K. Atsuki, and T. Hirahata, "Microstrip dispersion in a wide frequency range," *IEEE Trans. Microw. Theory Tech.*, Vol. 29, No. 6, 610–611, 1981.
5. Yamashita, E., K. Atsuki, and T. Ueda, "An approximate dispersion formula of microstrip lines for computer aided design of microwave integrated circuits," *IEEE Trans. Microw. Theory Tech.*, Vol. 27, No. 12, 1036–1038, 1979.
6. Krupka, J., "Frequency domain complex permittivity measurements at microwave frequencies," *Meas. Sci. Technol.*, Vol. 17, 55–70, Apr. 2006.
7. Kang, B., J. Cho, C. Cheon, and Y. Kwon, "Nondestructive measurement of complex permittivity and permeability using multilayered coplanar waveguide structures," *IEEE Microw. Wireless Compon. Lett.*, Vol. 15, No. 5, 381–383, May 2005.
8. Hinojosa, J., "*S*-parameter broadband measurements on-coplanar and fast extraction of the substrate intrinsic properties," *IEEE Microw. Wireless Compon. Lett.*, Vol. 11, No. 2, 80–82, Feb. 2001.
9. Queffelec, P., P. Gelin, J. Gieraltowski, and J. Loaec, "A microstrip device for the broadband simultaneous measurement of complex permeability and permittivity," *IEEE Trans. Magn.*, Vol. 30, No. 2, 224–231, Mar. 1994.
10. Ghodgaonkar, D. K., V. V. Varadan, and V. K. Varadan, "Free-space measurement of complex permittivity and complex permeability of magnetic materials at microwave frequencies," *IEEE Trans. Instrum. Meas.*, Vol. 39, No. 2, 387–394, Apr. 1990.
11. Mellegol, S. and P. Queffelec, "Extension and error analysis of the microstrip transmission-line method for the broad-band measurement of the permeability tensor," *IEEE Trans. Microw. Theory Tech.*, Vol. 54, No. 3, 1065–1075, Mar. 2006.
12. Bahadoor, A., Y. Wang, and M. Afsar, "Complex permittivity and permeability of hexaferrite and carbonyl iron powders using rectangular waveguide technique from 8.0–40.0 GHz," *Dig. IEEE Int. Magnetics Conf. INTERMAG Asia*, 891–892, Nagoya Congress Center, Japan, 2005.
13. Chen, L. F., C. K. Ong, C. P. Neo, V. V. Varadan, and V. K. Varadan, *Microwave Electronics Measurement and Material Characterization*, 291, John Willey and Sons, West Sussex, England, 2004.
14. Weir, W. B., "Automatic measurement of complex dielectric

constant and permeability at microwave frequencies," *Proc. IEEE*, Vol. 62, 33–36, 1974.

15. Barry, W., "A broad-band automated stripline technique for the simultaneous measurement of complex permittivity and permeability," *IEEE Trans. Microw. Theory Tech.*, Vol. 34, No. 1, 80–84, Jan. 1986.
16. Hu, J., A. Sligar, C. H. Chang, S. L. Lu, and R. K. Settaluri, "A grounded coplanar waveguide technique for microwave measurement of complex permittivity and permeability," *IEEE Trans. Magn.*, Vol. 42, No. 7, 1929–1931, Jul. 2006.
17. Azaro, R., F. Caramanica, and G. Oliveri, "Determination of the complex permittivity values of planar dielectric substrates by means of a multifrequency PSO-based technique," *Progress In Electromagnetics Research M*, Vol. 10, 83–91, 2009.
18. Ocera, A., M. Dionigi, E. Fratticcioli, and R. Sorrentino, "A novel technique for complex permittivity measurement based on a planar four-port device," *IEEE Trans. Microw. Theory Tech.*, Vol. 54, No. 6, 2568–2575, Jun. 2006.
19. Goodenough, J. B., *Magnetism and Chemical Bond*, 214, Willey, New York, 1963.
20. Altunyurt, N., M. Swaminathan, P. M. Raj, and V. Nair, "Antenna miniaturization using magneto-dielectric substrates," *Proc. IEEE Electronics Components and Technol. Conf.*, 801–808, Sep. 2009.
21. Mosallaei, H. and K. Sarabandi, "Magneto-dielectrics in electromagnetics: concept and applications," *IEEE Trans. on Antennas and Propagation*, Vol. 52, No. 6, 1558–1567, Jun. 2004.
22. Pozar, D. M., *Microwave Engineering*, 206, John Willey and Sons, 1998.
23. Wolff, I., *Coplanar Microwave Integrated Circuits*, 12, John Willey and Sons, 2006.
24. Ghione, G. and C. U. Naldi, "Coplanar waveguides for MMIC application: Effect of upper shielding, conductor backing, finite-extent ground planes, and line-to-line coupling," *IEEE Trans. Microwave Theory Tech.*, Vol. 35, No. 3, 260–267, 1987.
25. Wolff, I., *Coplanar Microwave Integrated Circuits*, 217, John Willey and Sons, 2006.
26. Wolff, I., *Coplanar Microwave Integrated Circuits*, 20, John Willey and Sons, 2006.
27. Simons, R. N., *Coplanar Waveguide Circuits, Components and Systems*, 94, John Willey and Sons, 2001.

28. Bedair, S. S. and I. Wolff, "Fast, accurate and simple approximate analytic formulas for calculating the parameters of supported coplanar waveguides for MMIC's," *IEEE Trans. Microw. Theory Tech.*, Vol. 40, No. 1, 41–48, Jan. 1992.
29. Hilberg, W., "From approximation to exact relations for characteristic impedances," *IEEE Trans. Microw. Theory Tech.*, Vol. 17, No. 5, 259–265, 1969.
30. Deka, J. R., N. S. Bhattacharyya, and S. Bhattacharyya, "Development of low cost automated PC-based insertion loss measurement setup using a simple source and detector in X-band," *IETE Tech. Rev.*, Vol. 22, 425, 2005.
31. Borah, S. and N. S. Bhattacharyya, "Synthesis and characterization of reduced size ferrite reinforced polymer composites," *AIP Proc. Int. Conf. on Magnetic Materials*, (Kolkata, India, Dec. 2007), Vol. 1003, 261–263, 2008.
32. Wu, M., X. Yao, and L. Zhang, "An improved coaxial probe technique for measuring microwave permittivity of thin dielectric materials," *Meas. Sci. Technol.*, Vol. 11, 1617–1622, 2000.
33. Griffiths, D. J., *Introduction to Electrodynamics*, 398–402, Prentice-Hall of India Pvt. Ltd., 1999.
34. Todd, M. G. and F. G. Shi, "Complex permittivity of composite systems: A comprehensive interphase approach," *IEEE Trans. on Diel. and Elect. Insul.*, Vol. 12, No. 3, 601–611, Jun. 2005.
35. Ku, H. S., J. A. R. Ball, E. Siores, and B. Horsfield, "Microwave processing and permittivity measurement of thermoplastic composites at elevated temperature," *Journal of Materials Processing Technology*, Vol. 89–90, 419–424, 1999.